SAND2020-2023J

Impacts on mechanical strength of chemical reactions induced by hydrous supercritical CO_2 in Boise Sandstone

R. Charles Choens II
1515 Eubank SE MS 0735
Albuquerque, NM 87185
Phone: (505) 845-9820
Fax: (505) 844-7354
rcchoen@sandia.gov

Impacts on mechanical strength of chemical reactions induced by hydrous supercritical CO_2 in Boise Sandstone

R. Charles Choens II[1*], Anastasia G. Ilgen[2], D. Nicolas Espinoza[3], Michael Aman[3], Jennifer Wilson[4], Thomas A. Dewers[1]

1. Sandia National Laboratories, Geomechanics Department, 1515 Eubank SE Mailstop 0750, Albuquerque, NM 87185-0750, United States
2. Sandia National Laboratories, Geochemistry Department, 1515 Eubank SE Mailstop 0754, Albuquerque, NM 87185-0754, United States
3. Department of Petroleum and Geosystems Engineering, The University of Texas at Austin, 200 E. Dean Keeton, Austin, TX 78712, United States
4. Akima Infrastructure Services, LLC, Albuquerque, NM

[*] Corresponding author. Email rcchoen@sandia.gov

Abstract

Geomechanics experiments were used to assess mechanical alteration of Boise Sandstone promoted by reactions with supercritical carbon dioxide ($scCO_2$) and water vapor. During geologic carbon storage, $scCO_2$ is injected into subsurface reservoirs, forming buoyant plumes. At brine-plume interfaces, $scCO_2$ can dissolve into native brines, and water from brines can partition into $scCO_2$, forming hydrous $scCO_2$. This study investigates the effect of hydrous $scCO_2$ on the strength of Boise Sandstone. Samples are first exposed to recirculating hydrous $scCO_2$ for 24 hours at 70°C and 13.8 MPa $scCO_2$ pressure. Samples are reacted with $scCO_2$ with added water contents up to 500 mL. After $scCO_2$ exposure, samples are deformed at room temperature under confining pressures of 3.4, 6.9, and 10.3 MPa. The results demonstrate that hydrous $scCO_2$ induces chemical reactions in Boise Sandstone, with ions migrating from the solid into the hydrous $scCO_2$ phase. At the longer time-scales, these reactions could lead to mechanical weakening in the samples; however, on the scale of our experiments, the strength changes are within sample variability. Because the solubility of water in $scCO_2$ is extremely low (0.008 mole H_2O per 1 mole CO_2), the mineral dissolution of Boise Sandstone was under 0.002 wt.%. Additionally, mineral grains and pore throats in Boise Sandstone are cemented with quartz, which is not susceptible to dissolution at these conditions. Our results indicate that humidity in $scCO_2$ plumes is unlikely to sustain chemical reactions and induce long term strength changes in quartz cemented sandstones due to resistant mineralogies and low water solubility.

63 **1. Introduction**

64 Geologic carbon storage (GCS) has been identified as a potential technology to offset
65 anthropogenic emissions of carbon dioxide (CO_2) to mitigate its greenhouse effects. The
66 reservoir pressure and temperature conditions of the target subsurface storage sites are such that
67 CO_2 is stable in its supercritical state, allowing for higher storage volumes. Over geologic
68 timescales, CO_2 dissolution into resident brines and precipitation of carbonate minerals ensure
69 CO_2 storage, if impermeable caprocks and structural/stratigraphic traps maintain sealing
70 integrity. To counter current emissions, an estimated 3.5 billion tons of CO_2 per year must be
71 sequestered [*Pacala and Socolow*, 2004; *Zoback and Gorelick*, 2012]. Each site must be capable
72 of storing large volumes of CO_2 over geologic time-scales, as well as sustaining large injection
73 rates during the injection phase. A major concern during injection would be geomechanical
74 hazards from altering in situ stress states during prolonged injection. Changes in stress states
75 could affect wellbore casing integrity, induce fractures, reactivate pre-existing faults, as well as
76 result in reservoir expansion and uplift at the surface [*Rutqvist*, 2012]. The development of
77 fractures in the storage or caprock lithologies threaten the safety and effectiveness of CO_2
78 storage operations. In this study we evaluate changes in the mechanical strength in Boise
79 Sandstone in response to CO_2 injection. Sandstones are typical target lithologies for CO_2 storage
80 in saline formations.

81 Once injected, supercritical CO_2 ($scCO_2$) disrupts the chemical equilibrium between brine
82 and mineral assemblages in the subsurface. In the presence of water, CO_2 forms carbonic acid,
83 lowering the pH of the brines, and induces dissolution/precipitation reactions. At low pH values,
84 CO_2 brines can dissolve carbonates and silicate minerals [*Huq et al.*, 2015; *Koide et al.*, 1993;
85 *Lamy□Chappuis et al.*, 2014; *Rosenbauer et al.*, 2005]. Decreasing pH due to carbonic acid

86 formation can promote the dissolution of feldspars [*J Lu et al.*, 2014; *P Lu et al.*, 2011; *Tutolo et*
87 *al.*, 2015], zeolites, micas, and clay minerals [*Alemu et al.*, 2011; *Credoz et al.*, 2011; *Garcia et*
88 *al.*, 2012; *Kim et al.*, 2011; *Liu et al.*, 2012; *Luquot et al.*, 2012; *Shao et al.*, 2010], resulting in
89 the deposition of carbonate phases and amorphous silica. Experiments on carbonate-cemented
90 rocks have demonstrated drastic mechanical weakening at low pH conditions caused by CO_2
91 dissolution in brine [*Castellanza and Nova*, 2004; *Ciantia et al.*, 2015; *Ciantia and Hueckel*,
92 2013; *Gajo et al.*, 2015; *Hangx et al.*, 2009; *Le Guen et al.*, 2007]. Consequently, in calcite
93 bearing sandstones with no reactive grain cements, dissolution reactions have a negligible effect
94 on strength [*Hangx et al.*, 2013]. In lithologies lacking reactive minerals, experiments have
95 shown no alterations in strength following the reaction with CO_2-acidified brines [*Hangx et al.*,
96 2010; *Le Guen et al.*, 2007]. In alkaline waters, CO_2-acidified brines can precipitate carbonate
97 minerals, possibly increasing strength [*Rosenbauer et al.*, 2005].
98 Due to heterogeneity in composition and fabric of target storage formations, predicting
99 potential chemical reactions triggered by CO_2 injection and the resulting changes in
100 geomechanical properties is extremely difficult. Chemical reactions can dissolve both cementing
101 and framework minerals, which could lead to a decrease in strength. Similarly, alteration
102 reactions of stronger minerals to weaker minerals, as well as density contrast between the parent
103 and altered phases, could also lead to decreases in strength. Precipitating new minerals at grain
104 contacts could increase strength, but deposits around pore linings would likely have a negligible
105 effect on strength. Previous work has focused on $scCO_2$ dissolved into aqueous solutions with
106 the aqueous phase not being limited in volume. In this paper we examine how humid $scCO_2$
107 interacts with sandstone. In this case, the volume of the aqueous phase is limited, which is
108 representative of a scenario when a humid $scCO_2$ plume (as opposed to CO_2-acidified brine)

travels in the subsurface. Water molecules partition into $scCO_2$ plumes, which results in a humid $scCO_2$. This humid $scCO_2$ phase can possibly form a concentrated acid that could condense at the pore throats, enhancing mineral dissolution there. The goal of this study is to evaluate the changes in strength due to chemical reactions induced by water present as a vapor phase in hydrous $scCO_2$. Experiments are conducted on Boise Sandstone, a clay rich sandstone with 29% porosity and published permeability values on the order of $1.5x10^{-12}$ m^2 [*Zhu and Wong*, 1997]. Hydrous $scCO_2$ is recirculated through the sample prior to geomechanical strength tests to induce chemical reactions. Experiments are conducted at a range of confining pressures, relevant to GCS conditions, to investigate induced chemical reactions and resulting changes in mechanical strength.

2. Methods

2.1. Sample Description

Experiments were conducted on Boise Sandstone, a porous clastic sandstone from the Upper Miocene Idaho Formation. Samples were cored from larger blocks taken from outcrops. X-ray diffraction analysis shows that Boise Sandstone consists of 31 % quartz, 28% albite, 17% microcline, 15% illite-smectite, and 9% calcite, by weight [*Major*, 2018]. Measured porosity is 29%. Photomicrographs of samples show that grains and pore throats are coated with microcrystalline quartz and quartz overgrowths. Fine grained matrix found between grains contains incipient quartz cementation (Figure 1). Samples are cylindrical, 25.4 mm in diameter and 50±2.5 mm in length. Samples were maintained at 0-40% humidity and temperatures between 20 and 25°C. Samples were sonicated in isopropanol to remove any fines from coring and allowed to dry prior to exposure to $scCO_2$, and end-face ground prior to axial deformation. Additional discs of Boise Sandstone 6.35±2.5 mm in length were prepared from 25.4 mm diameter cores.

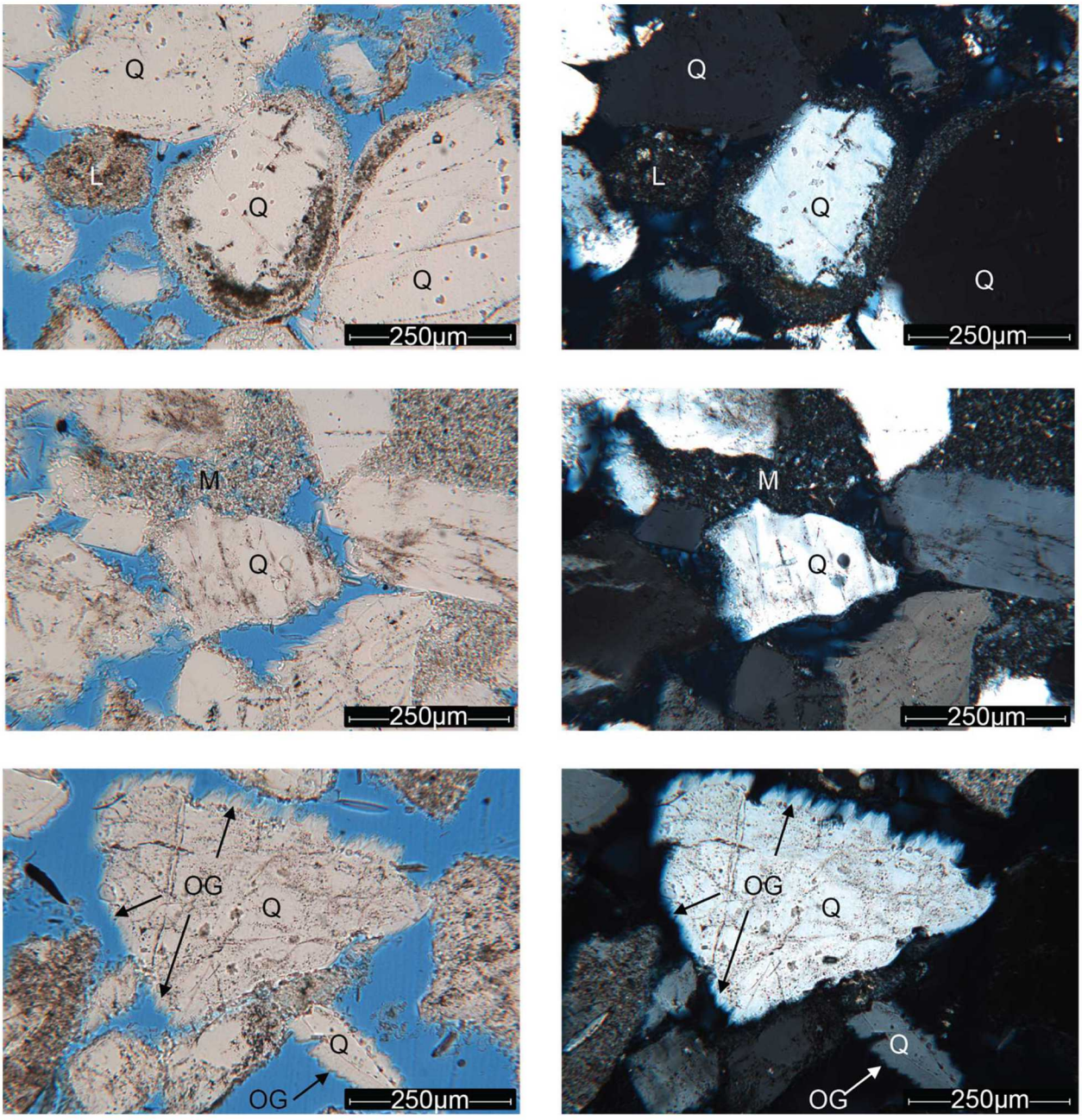

Figure 1. Photomicrographs of Boise Sandstone. Left column is images taken under plane light, right column is images taken under plane polarized light. Images show quartz grains (Q), lithic fragments (L), fine grained matrix (M), and quartz overgrowths (OG).

2.2. Exposure to supercritical CO_2

Samples were exposed to dry $scCO_2$ and $scCO_2$ with different added water content and subsequently tested at room temperature conditions in a separate load frame. Hydrous $scCO_2$ was generated in a 2.5L titanium reaction vessel. The vessel was filled with UHP-grade liquid CO_2, heated to 70°C, and pressurized to 13.8 MPa to convert CO_2 to a supercritical state. De-ionized Milli-Q water with a resistivity of 18 MΩ, DI H_2O, was added to the vessel via a high pressure liquid chromatography injector valve and a recirculating pump. DI H_2O was added in 5mL increments for successive experiments. At 13.8 MPa and 70°C, the mole fraction of water soluble in CO_2 is 0.82% [*Spycher et al.*, 2003], which corresponds to a volume of 3.6 mL in 2.5L $scCO_2$. Because the solubility of DI H_2O in $scCO_2$ is so low, available water should be the limiting factor for chemical reactions. We conducted our experiments with excess water in the system to understand if increasing water availability could maintain chemical reactions over more restricted environments. Experiments were conducted with 0, 5, 10, 15, 20, 25, 30, 35, and 40 mL added DI H_2O. Additional experiments were conducted with 500 mL of DI H_2O added into the reaction vessel prior to the addition of liquid CO_2 to ensure available water in excess of the pore volume for Boise Sandstone.

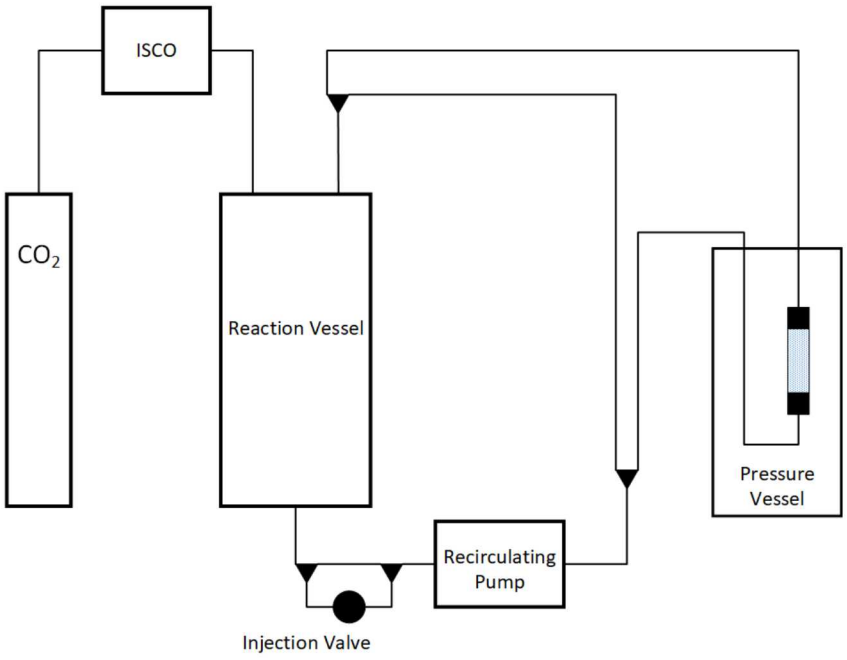

Figure 2. Plumbing schematic for exposing Boise Sandstone samples to hydrous $scCO_2$. Black triangles represent 3-way, 2-stem valves to change flow paths. 2-way valves, heaters, and pressure relief devices omitted for clarity.

Boise Sandstone samples were pressurized in a separate hydrostatic vessel (Figure 2). Both the sandstone cores and discs were reacted in series during an experiment where the disc is on the upstream side, separated from each other and the endcaps by Hastelloy frits. The sample stack was isolated from the confining pressure medium using a two-layer jacketing procedure. A 0.05 mm annealed nickel foil jacket was wrapped around the sample and covered by an outer layer of heat shrink PTFE tubing. The jackets were affixed to the endcaps using nichrome wire and UV cure urethane. The hydrostatic vessel with the sample was heated to 70°C and pressurized to 15.5 MPa during the $scCO_2$ exposure to maintain 1.7 MPa effective pressure, P_E, (15.5 MPa confining pressure, P_C, - 13.8 MPa pore pressure, P_P). $scCO_2$ was circulated through the sample stack using a recirculating pump that pulled $scCO_2$ from the top of the reaction

vessel, through the sample stack, and back into the reaction vessel via a port in the bottom, minimizing the chance for accidental back flow of liquid water into the sample while allowing $scCO_2$ to re-equilibrate with water after flowing through the sample (Figure 2). Water present in $scCO_2$ was able to interact with Boise Sandstone and precipitate/redissolve in pore spaces with $scCO_2$ flow. Samples were exposed for 24 hours, and an additional sample was exposed to $scCO_2$ with 500 mL DI H_2O for 168 hours to investigate time effects. After exposure, samples were isolated, and the recirculating pump and heaters were stopped. The sample was removed from the hydrostatic vessel for mechanical testing in a separate load frame. After cooling and depressurization, DI H_2O condensed out of $scCO_2$ and collected with the excess water at the bottom of the reaction vessel that was sampled for quantifying ion concentration using an inductively coupled plasma mass spectrometer (ICP-MS) and ion chromatography (IC). Collected fluids were filtered using a 0.45 μm Whatman filter with nylon membrane, and then diluted by a factor of three with deionized water. Half of the samples were then acidified with 6 N ultrapure nitric acid at a ratio of 1 mL nitric acid per 100 mL sample for cation analysis. The remaining samples were used for anion analysis. In between experiments, the reaction vessel and pore lines were triple rinsed using DI H_2O; any ions detected in solution after experiments were carried from the sandstone sample by hydrous $scCO_2$ as a result of an aqueous phase reacting with the sample during exposure.

2.3. Triaxial Testing

Boise Sandstone cores were tested in two different triaxial load frames: a Hassler style triaxial core holder and a 978 kN servo hydraulic MTS load frame. Axial loading and confining pressure in the coreholder are delivered by separate syringe pumps. The sample was isolated

195 from the confining pressure via a viton sleeve. In the 978 kN frame, the sample was jacketed
196 with heat shrink poly-olefin tubing. Use of this frame allowed radial strain to be measured using
197 a 5 mm LVDT mounted to the sample to calculate elastic moduli from unload-reload loops in
198 order to compare small variations in mechanical properties due to incremental added water for
199 experiments conducted at 6.9 MPa P_C; it was not possible to measure elastic moduli for samples
200 deformed in the coreholder. Unaltered samples and samples exposed to $scCO_2$ with 500 mL DI
201 H_2O were axially loaded at 0, 3.4, 6.9, 10.3 MPa P_C. Samples exposed to 0 – 40 mL added DI
202 H_2O were deformed at 6.9 MPa P_C. Samples were deformed at an axial strain rate of 10^{-5} sec^{-1}.
203 Triaxial experiments were conducted dry and at room temperature. One unconfined compressive
204 strength, UCS, experiment was performed without confining pressure on a water saturated
205 sample, and an additional experiment was performed where DI H_2O was flowed through an
206 unaltered sample at 0.2 mL/min at 70°C under an effective pressure of 6.9 MPa (20.7 MPa P_C
207 minus 13.8 MPa P_P) to investigate water and temperature effects on strength.
208
209 *2.4. Scratch Testing*
210 The reacted discs were scratch tested to measure changes in elastic properties with $scCO_2$
211 exposure. An 80.1 N normally loaded indenter was displaced at a constant rate across the sample
212 face. Post deformation, scratches were photographed using an optical microscope and measured
213 using the MATLAB Image Processing Toolbox (Figure 3) [*Aman et al.*, 2018]. The geometry of
214 the induced scratch and shear force during the experiments can be used to calculate scratch
215 toughness and scratch hardness. The scratch hardness, $H_{Scratch}$, is calculated according to ASTM
216 G171:
217 $$H_{Scratch} = \frac{kF_v}{w^2},$$

where F_v is the normal force, w is the average scratch width, and $k = 24.98$ is a geometric constant for the indenter tip. Scratch toughness, K_C, is calculated as

$$K_C = \frac{F_T}{\sqrt{f(w)}},$$

where

$$f(w) = 2(2R\sin^{-1}\left(\frac{w}{2R}\right))(R^2\sin^{-1}\left(\frac{w}{2R}\right) - \frac{wR}{2}\cos\left(\sin\left(\frac{w}{2R}\right)\right)),$$

where F_T is the shear force, p is the scratch perimeter, and R is the radius of the probe tip (200 μm).

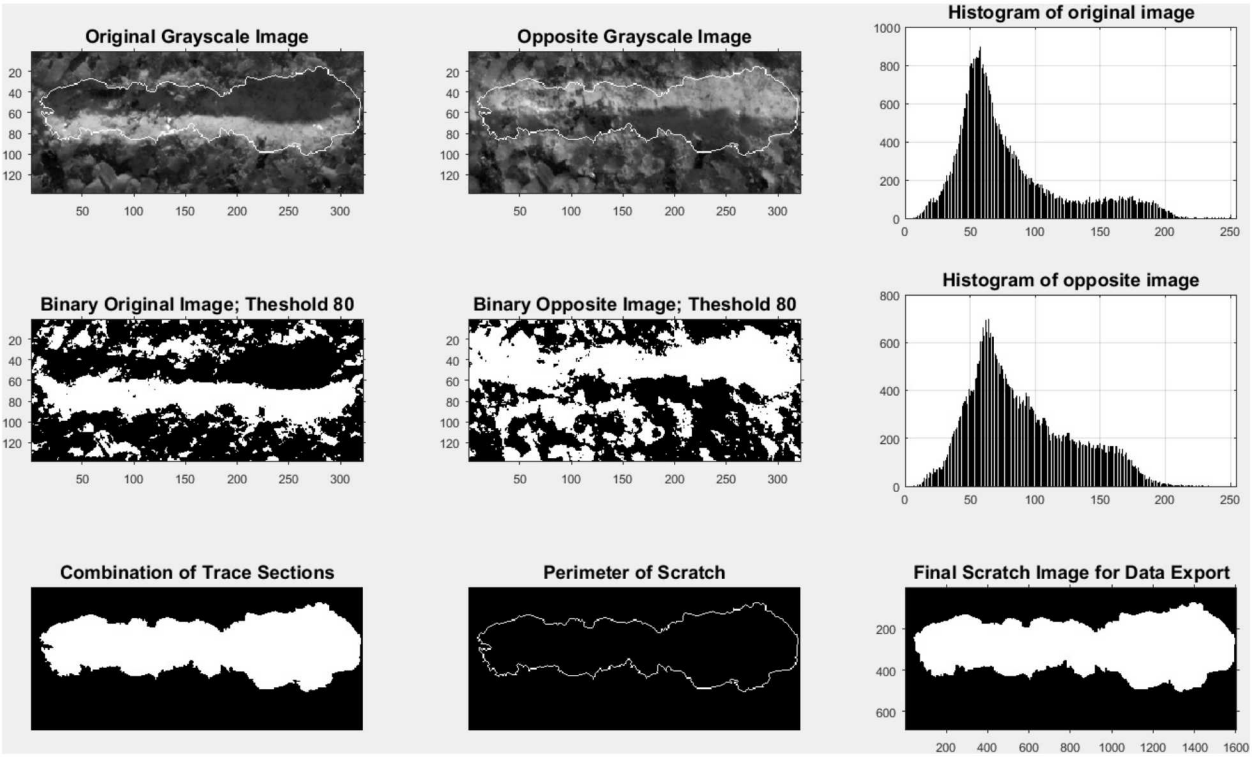

Figure 3. Scratch analysis from Boise Sandstone sample exposed to dry $scCO_2$. MATLAB image analysis tool used to calculate the perimeter of the scratch. Length unit in photos is 10^{-6} m.

231 *2.5. Geochemical Modeling*

232 The Geochemist Workbench (GWB) software [*Bethke*, 2008] was used for reaction path
233 modeling (React module). Reaction path modeling was used to predict solution composition as a
234 function of reaction progress and volume of water added to $scCO_2$ prior to reacting with Boise
235 Sandstone. The modeling input, including kinetic rate parameters, is listed in Table 1. The
236 reaction was set to proceed for 24 hours, to match the experiments. Two models with lower
237 water contents (5 and 10 mL of H_2O) were run for 10,000 years to test the reactivity of the
238 system over geological storage timescales. We used the Lawrence Livermore National
239 Laboratory (LLNL) thermo.dat database included in the GWB package. The CO_2 fugacity was
240 fixed at 136 atm for all tested cases to match experimental conditions (13.8 MPa), and
241 temperature was set at 75 °C. The solid to liquid ratio in the models matched that of the
242 experiments. High temperature phases (e.g., tridymite) were suppressed.

243
244 Table 1. Input data for the reaction path models. Temperature was set at 75°C for all cases.
245 Volume of H_2O was varied from 5 mL to 500 mL, to match the experiments.

Minerals	Mass (g)	Surface area ($cm^2\ g^{-1}$)	Kinetic rate constant (mol $cm^{-2}\ s^{-1}$)
Quartz	15.5	3	1.02×10^{-18}
Albite	14.0	5	1.44×10^{-12}
K-feldspar	8.5	3	3.89×10^{-17}
Calcite	4.5	3	1.00×10^{-11}
Illite	7.5	3	1.66×10^{-14}

246

3. Results and Discussion

All tested samples failed by the development of a through going inclined fracture, consistent with dilatant shear failure characterized by the Mohr-Coulomb failure criterion (Figure 4). Weakening is observed in samples exposed to hydrous $scCO_2$, but the effect of increasing water availability is not consistent for all conditions tested (Figure 5,6; Table 2). Scratch testing results do not elucidate the relationship between observed weakening and added water (Figure 7; Table 3). Water collected post-exposure contains measurable ion concentrations, indicating mineral dissolution by the humid $scCO_2$ phase (Figure 8; Table 4).

3.1. Triaxial Testing Results

Control experiments demonstrate that Boise Sandstone fails at similar differential stress levels in both load frames (Figure 6c). Obvious differences are apparent in the post failure response between the two frames. Because the 978 kN frame is much stiffer than the coreholder, there are apparent differences between sample responses due to varying amounts of frame stretch. Samples deformed in the 978 kN frame display a sharp stress drop after failure, while samples deformed in the coreholder strain significantly post failure as the coreholder elastically unloads. Sample loading is stiffer in the 978 kN frame as well, and elastic moduli are only reported for experiments in the 978 kN frame (Table 2). For experiments on unaltered samples conducted at four different confining pressures, the peak differential stress can be described by a linear failure envelope (Figure 6, 7d).

Table 2. List of experiments with exposure time, added water volume, triaxial testing conditions, measured elastic moduli, and failure strength.

270

	P_C (MPa)	Water Added (mL)	Peak $\Delta\sigma$ (MPa)	E (GPa)	ν	Exposure Time (Hours)
Control Experiments						
UCS	0	---	31.0	---	---	---
Wet UCS	0	Saturated	30.0	---	---	---
Dry 3.4 MPa	3.4	---	34.5	---	---	---
Dry 6.9 MPa 1	6.9	---	57.1	---	---	---
Dry 6.9 MPa 2	6.9	---	56.0	---	---	---
Dry 6.9 MPa 3	6.9	---	54.2	8.44	0.1	---
Dry 10.3 MPa	10.3	---	72.1	---	---	---
Wet 6.9 MPa*	6.9	Saturated	57.4	---	---	---
Dry $ScCO_2$ 6.9 MPa	6.9	---	58.6	---	---	24
Hydrous $scCO_2$						
+ 5 mL DI H_2O	6.9	5	60.2	---	---	24
+ 10 mL DI H_2O	6.9	10	61.1	---	---	24
+ 15 mL DI H_2O	6.9	15	57.1	8.41	0.12	24
+ 20 mL DI H_2O	6.9	20	47.7	7.95	0.12	24
+ 25 mL DI H_2O	6.9	25	51.9	8.17	0.1	24
+ 30 mL DI H_2O	6.9	30	53.4	8.31	0.12	24
+ 35 mL DI H_2O	6.9	35	53.3	8.51	0.12	24
+ 40 mL DI H_2O	6.9	40	59	7.94	0.13	24
Excess Wet CO_2 3.4 MPa	3.4	500	47	---	---	24
Excess Wet CO_2 6.9 MPa	6.9	500	49.2	---	---	24
Excess Wet CO_2 10.3 MPa	10.3	500	53.1	---	---	24
Excess Wet CO_2 1 week	6.9	500	56.3	---	---	168

*Experiment conducted at 70°C and flow rate of 0.2 ml/min

271
272

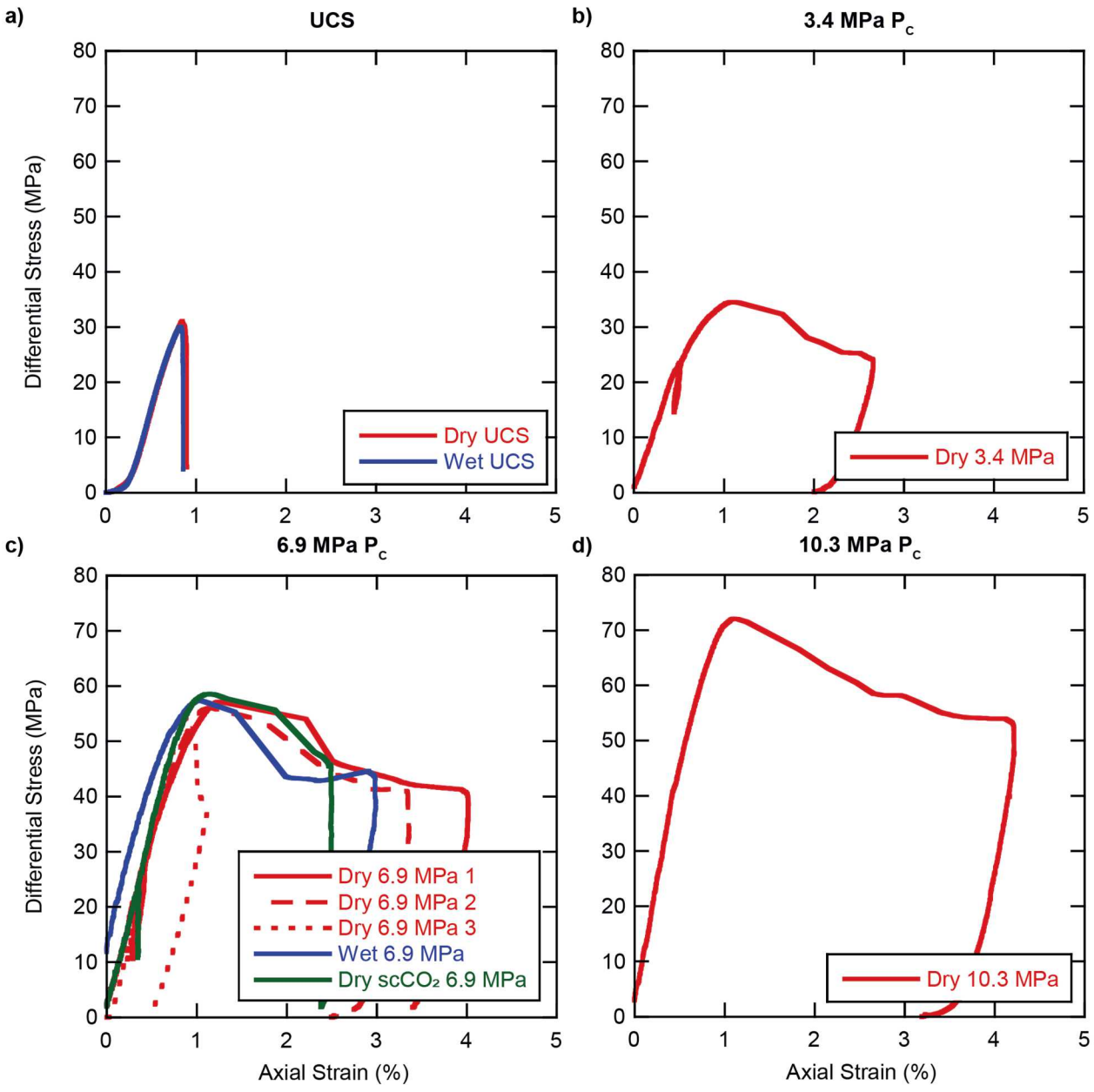

Figure 4. Differential stress versus axial strain for experiments conducted a) unconfined, b) at 3.4 MPa P_C, c) at 6.9 MPa P_C, and d) at 10.3 MPa P_C.

Experiments were conducted on Boise Sandstone samples saturated with DI H_2O to separate possible water weakening effects from potential changes in strength due to chemical reactions induced by hydrous $scCO_2$. Loading response and failure strength in UCS tests are

280 similar for unaltered and DI H_2O saturated samples (Figure 4a). The loading response and
281 failure for a sample deformed at 70°C in the presence of flowing DI H_2O is similar to unaltered
282 samples (Figure 4c). Samples exposed to dry $scCO_2$ for 24 hours do not show significant
283 changes in strength.
284 Samples exposed to $scCO_2$ with 500 mL added DI H_2O demonstrate drastically different
285 results when deformed at different confining pressures (Figure 5). At 3.4 MPa P_C, the sample
286 exposed to $scCO_2$ with excess DI H_2O is stronger than the unaltered sample, though this could be
287 in part due to natural variability in strength (Figure 5a). At higher confining pressures, the
288 samples exposed to $scCO_2$ with excess DI H_2O show significant weakening compared to
289 unaltered samples. At 6.9 MPa P_C, the loading response is similar, only the failure strength is
290 reduced (Figure 5b). At 10.3 MPa P_C, both the loading response and the failure strength are
291 reduced in the sample exposed to hydrous $scCO_2$ (Figure 5c). The changes in failure strength
292 alter the failure envelope, and samples exposed to hydrous $scCO_2$ have a much lower slope for
293 failure versus mean stress, but altered samples have a higher y-intercept. As mean stress
294 increases, failure strength decreases with exposure (Figure 5d).
295

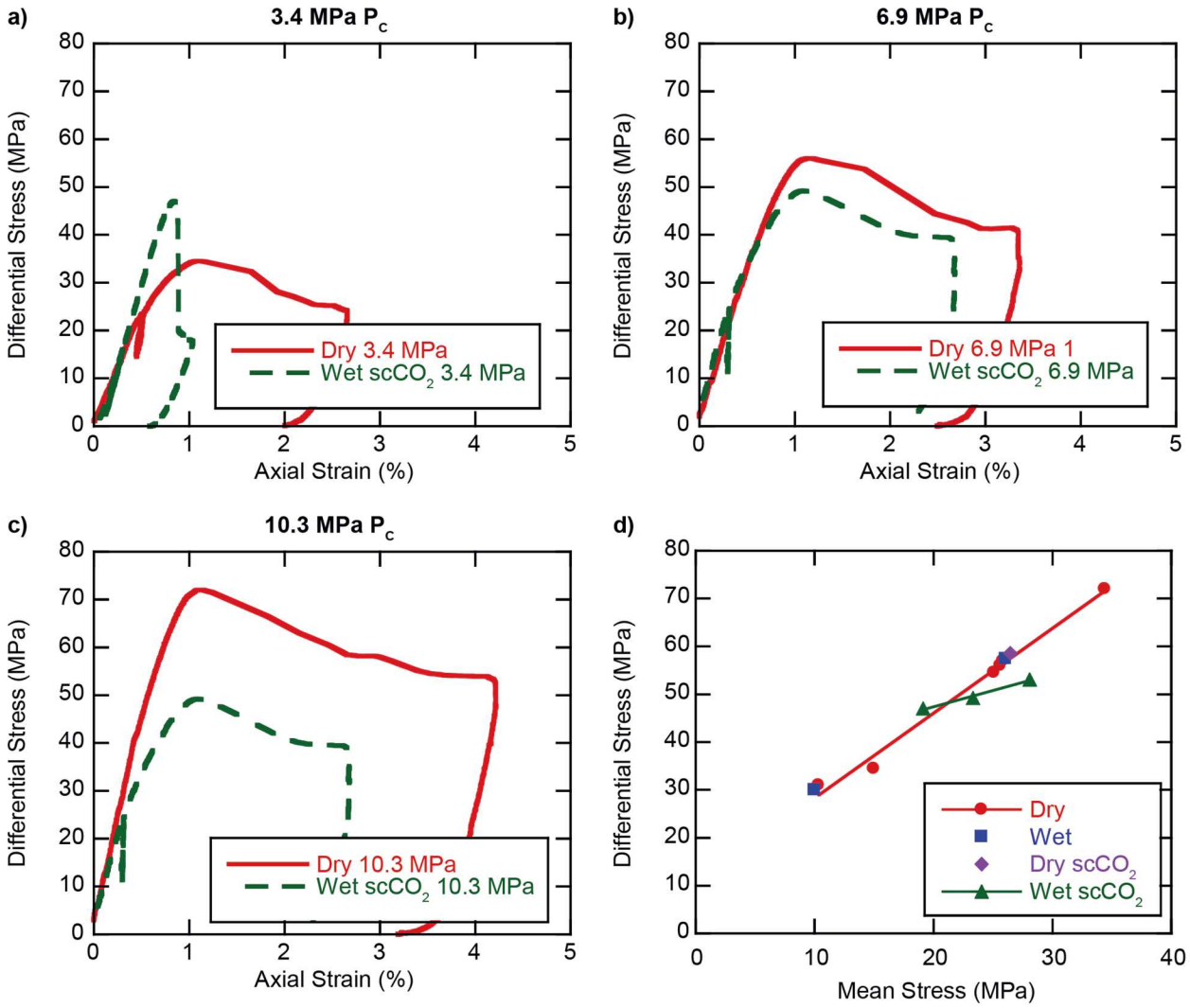

296

297 Figure 5. Differential stress versus axial strain for experiments on unaltered and samples
298 exposed to $scCO_2$ with 500 mL added DI H_2O conducted a) at 3.4 MPa P_C, b) at 6.9 MPa P_C, c)
299 at 10.3 MPa P_C, and d) peak differential stress versus mean stress. Axial stress resolution is 0.2
300 MPa for both frames, and standard deviation from control experiments at 6.9 MPa P_C is less than
301 2%.

302

303 Samples exposed to $scCO_2$ with up to 40 mL added DI H_2O were deformed at 6.9 MPa
304 P_C. Weakening was observed in the presence of humid $scCO_2$, but there is no correlation with
305 volume of added DI H_2O to the system (Figure 6). At low water contents, samples show slight

306 strengthening compared to unaltered samples. At 20 mL added DI H_2O, there is a decrease in
307 strength. With increasing DI H_2O, there are smaller decreases in strength compared to unaltered
308 samples. The sample exposed to $scCO_2$ with 40 mL added DI H_2O shows strengthening, and the
309 sample exposed to $scCO_2$ with 500 mL added DI H_2O shows a decrease in strength. While
310 exceeding the standard deviation of the repeated control experiments on dry samples at 6.9 MPa
311 P_C, 2%, the observed changes in strength with added water are a small percentage of the
312 unaltered failure strength (<10%), and the relationship between failure strength and added water
313 levels is not consistent, (Figure 6a; Table 2). Changes in elastic moduli also do not correlate
314 with the added volumes of water. Young's modulus decreases with exposure to hydrous $scCO_2$,
315 but the results show less than a 6% decrease. Poisson's ratio increases and is uniformly elevated
316 for all water contents (Figure 6b).
317

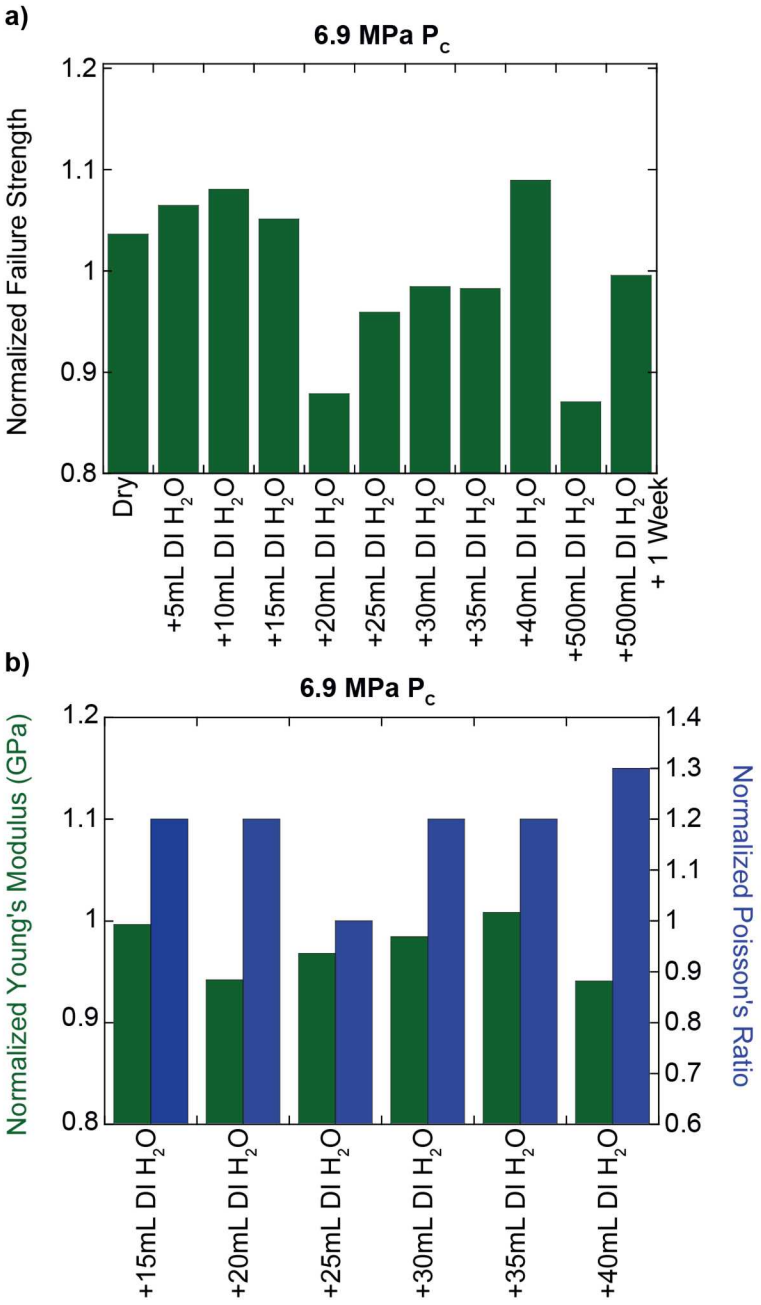

Figure 6. Mechanical results for experiments conducted at 6.9 MPa P_C exposed to hydrous $scCO_2$. a) Peak differential stress for different water contents normalized by the failure strength for unaltered samples. b) Young's modulus and Poisson's ratio for different water contents normalized by values for unaltered samples.

3.2. Scratch Test Results

Discs exposed to hydrous $scCO_2$ were scratch tested using an 80.1 N normally loaded indenter displaced across the surface at a constant rate. Photographs, measurements, and analysis for individual samples are listed in Supplemental Material. Scratch toughness measurements show weakening with exposure, but the relationship with water content is not consistent (Figure 7a; Table 3). The greatest weakening is observed at 5 mL added DI H_2O. With increasing water content, samples are weaker compared to unaltered samples; however, these differences may not be significant given the scale of standard deviation for these measurements. Samples altered in $scCO_2$ with 20 and 25 mL added DI H_2O are weaker than unaltered samples, but all other water contents are within experimental measurement error for unaltered samples. Hardness measurements are similar to scratch toughness measurements, except the variability is less for hardness measurements (Figure 7b; Table 3). The greatest weakening is still observed at 5 mL added DI H_2O, and clear weakening trend is observed for samples altered at 20-40 mL added DI H_2O. The relationship between the observed weakening and water content is not consistent.

Table 3. Results for scratch testing on samples exposed to hydrous $scCO_2$.

	Scratch Hardness (GPa)	Standard Deviation	Scratch Toughness (MPa $m^{0.5}$)	Standard Deviation
Dry	0.3	0.061	2.6	0.834
+ 5 mL DI H_2O	0.05	0.013	0.55	0.169
+ 10 mL DI H_2O	0.18	0.094	1.85	0.823
+ 15 mL DI H_2O	0.25	0.105	2.25	0.704
+ 20 mL DI H_2O	0.09	0.046	1.06	0.45
+ 25 mL DI H_2O	0.09	0.024	1.1	0.397
+ 30 mL DI H_2O	0.16	0.051	1.58	0.461
+ 35 mL DI H_2O	0.16	0.035	1.54	0.203
+ 40 mL DI H_2O	0.12	0.046	1.46	0.607

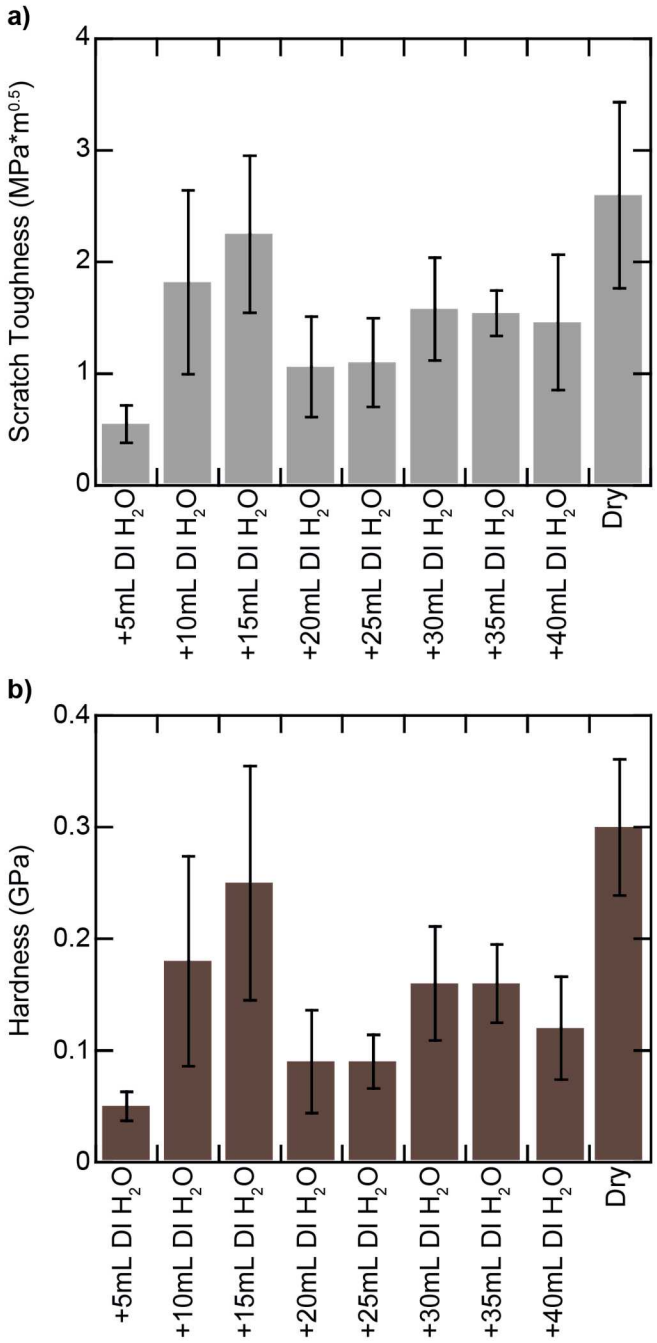

Figure 7. Scratch testing results. a) Scratch toughness and b) hardness for samples exposed to different humidity $scCO_2$. Black bars show 1 standard deviation.

3.3. Geochemical Analysis Results

After exposure, any water condensed out of hydrous $scCO_2$ during cooling and depressurization was sampled for ion concentration measurements using an IC and ICP-MS. Measurable ion concentrations are detected in all samples. In between experiments, the reaction vessel and pore lines were triple rinsed using DI H_2O; during experiments, the flow path was designed to prevent exposing the sample to liquid water; post-exposure, the sample was isolated from the reaction vessel during cooling and depressurization. Ions detected in solution after experiments indicate that an aqueous phase was in contact with the core sample during exposure and measured ions were carried by hydrous $scCO_2$.

The highest concentration of ions observed in solution is sodium, Na^+, calcium, Ca^{2+}, and potassium, K^+ (Figure 8a; Table 4). Magnesium, Mg^{2+}, iron, Fe, aluminum, Al and silica, Si, are present at lower concentrations (Figure 7b; Table 4). In $scCO_2$ with 5 mL DI H_2O, Ca^{2+} to Na^+ ratio is the highest observed, and it decreases with increasing water content. Both Na^+ and Ca^{2+} are present in higher concentrations than K^+ except for some of the tests at higher water content. Observed Fe is higher than Mg^{2+} for all conditions except at added 30 mL DI H_2O (Figure 8b; Table 4). Fe concentrations decrease with increasing water, but spike for $scCO_2$ with 500 mL DI H_2O (Figure 8b; Table 4). Elevated Fe levels could have resulted from interactions with pore lines, but Fe concentrations do not increase with increasing exposure time and decrease with added water up to 40 mL, suggesting that vessel and line corrosion was not significant. Aluminum concentrations are low and stable throughout the experiments. Silicon concentrations vary, but do not depend on water content (Figure 8b; Table 4). Silicon concentrations spike at 5 and 30 mL added DI H_2O, but are otherwise near 1 mg/L and fall in between Fe and Mg^{2+}.

With increasing water volume added to $scCO_2$, concentrations of ions decrease (Figure 8). Total dissolved solids, TDS, remain at a low level for all tests. Total dissolved solids vary

between 1 mg/L and 214 mg/L, depending on the water content. At low water contents, the concentration does not depend on increasing water volume in the system. At the highest water contents, TDS values are lowest and decrease with increasing water and exposure time. The mass of dissolved rock can be calculated using TDS and the volume of water added to the system (Figure 8c; Table 4). The percentage of rock dissolved is low for all experiments, varying between 0.5 mg and 4 mg (while the sample weighs 50 grams on average). Values spike at 15, 35, and 500 mL added DI H_2O, but values are otherwise ~1 mg (Figure 8c). Dissolved rock decreases with exposure time in $scCO_2$ with excess DI H_2O.

Since our alteration experiments were short-term (24 to 168 hours), and mineral dissolution is kinetically-controlled, we constructed geochemical models to predict the long-term trends in mineral dissolution and precipitation in Boise Sandstone lithology.

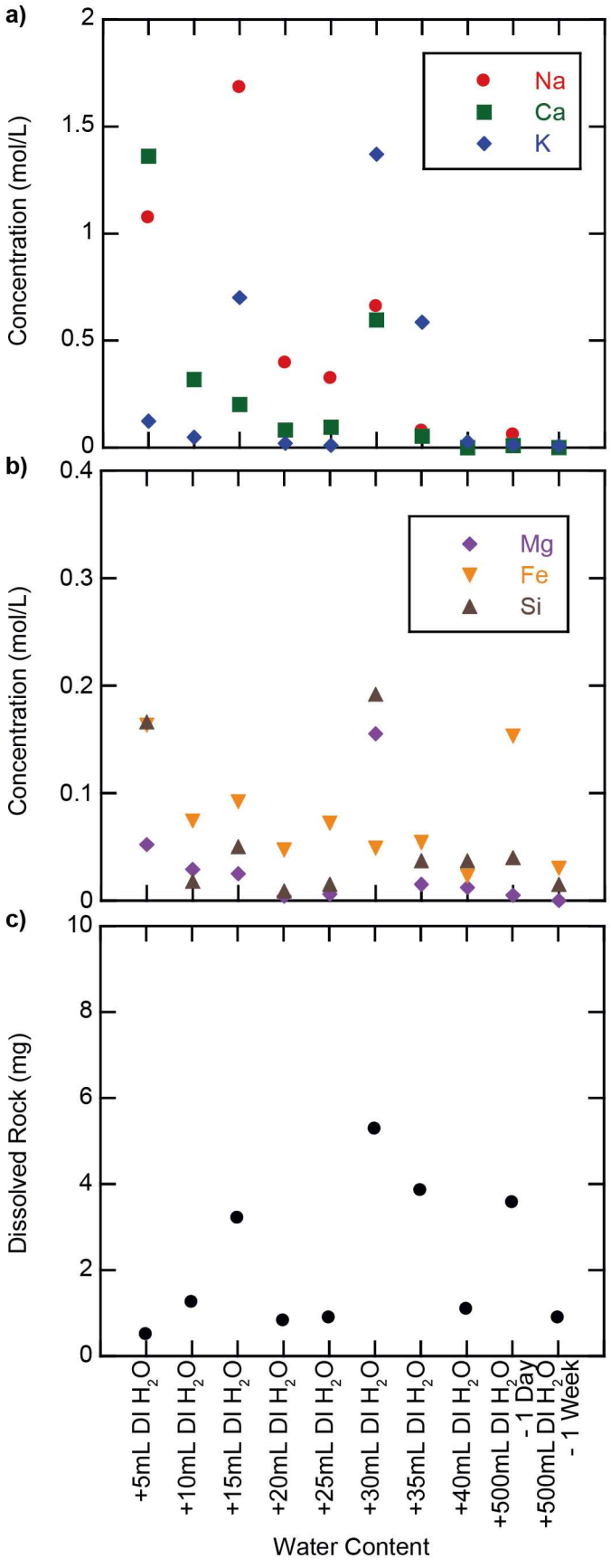
a)
Concentration (mol/L)
Na
Ca
K
b)
Concentration (mol/L)
Mg
Fe
Si
c)
Dissolved Rock (mg)
+5mL DI H2O
+10mL DI H2O
+15mL DI H2O
+20mL DI H2O
+25mL DI H2O
+30mL DI H2O
+35mL DI H2O
+40mL DI H2O
+500mL DI H2O - 1 Day
+500mL DI H2O - 1 Week
Water Content

383

Figure 8. Measured ion concentration after exposure at different added water content. a) Concentration of sodium, calcium, and potassium. b) Concentration of magnesium, iron, and silica. c) Calculated mass of dissolved rock based on measured ion concentrations.

Table 4. Measured concentration of ions in solution post-exposure.

	Na (mmol/L)	Ca (mmol/L)	K (mmol/L)	Mg (mmol/L)	Si (mmol/L)	Al (mmol/L)	Fe (mmol/L)	TDS (mg/L)	Dissolved Rock (mg)
+ 5 mL DI H_2O	1.07	1.36	0.12	0.05	0.17	0.01	0.16	99.02	0.50
+10 mL DI H_2O	2.47	0.32	0.05	0.03	0.02	0.01	0.07	125.42	1.25
+15 mL DI H_2O	1.68	0.20	0.70	0.02	0.05	0.01	0.09	213.86	3.21
+20 mL DI H_2O	0.40	0.08	0.02	0.00	0.01	0.02	0.05	40.85	0.82
+25 mL DI H_2O	0.32	0.09	0.01	0.01	0.02	0.02	0.07	35.66	0.89
+30 mL DI H_2O	0.66	0.60	1.37	0.15	0.19	0.01	0.05	175.86	5.28
+35 mL DI H_2O	0.08	0.05	0.58	0.01	0.04	0.02	0.05	109.90	3.85
+ 40 mL DI H_2O	0.00	0.00	0.03	0.01	0.04	0.01	0.02	27.37	1.09
Excess Wet CO_2 6.9 MPa	0.06	0.01	0.01	0.01	0.04	0.01	0.15	7.14	3.57
Excess Wet CO_2 1 week	0.00	0.00	0.01	0.00	0.01	0.01	0.03	1.65	0.89
Detection limit, mmol/L	0.9×10^{-3}	2.5×10^{-3}	0.5×10^{-3}	0.8×10^{-3}	2.1×10^{-3}	0.2×10^{-3}	0.09×10^{-3}		
RSD (%)	1.9	2.2	1.4	2.2	5.0	1.8	2.9		

391 *3.4 Geochemical Modeling Results*

392 To model the chemical reactions which would take place if Boise Sandstone was reacted
393 with humid $scCO_2$ on storage time scales, we constructed geochemical models, using our
394 experimental measurements. The mass of the minerals present in the solid core is known, based
395 on X-ray diffraction analysis [*Major*, 2018]. However, the accessible surface area for each
396 mineral is uncertain. The initial mineral dissolution rates were chosen to match those reported in
397 the CO_2-storage literature [*Xu et al.*, 2010]. However, we adjusted the dissolution rates for calcite
398 and albite, to improve the agreement between the model and Ca^{2+}, Na^{+}, Si, and Al aqueous
399 concentrations we observed in the tested systems (Figure 9a, b; Table 1). Dissolution rate for
400 albite in our models is ~ 2 orders of magnitude faster compared to previously reported values
401 [*Chen and Brantley*, 1997]. This could be due to either (1) faster dissolution of albite in hydrous
402 $scCO_2$, compared to aqueous systems, or (2) other potential sources of Na^{+} ion in our systems,
403 for example residual brine.

404 These models were used to predict the long-term response of Boise Sandstone to the
405 injection of CO_2. We extended the reaction time to 10,000 years. Our results indicate that
406 mineral dissolution and precipitation are predicted at the time scales of geological carbon
407 storage. New phases predicted to precipitate are amorphous silica, dolomite, kaolinite,
408 pyrophyllite, and muscovite (Figure 9c). Preexisting framework grains are largely unaffected;
409 only illite has significant dissolution over time. The total change in mineral mass is an increase
410 of ~ 0.3% (Figure 9d), and such a small change in mass should not lead to significant changes in
411 reservoir rock properties in a sandstone with resistant quartz linings and overgrowths. Porosity
412 and rock strength will be largely unaffected by the changes. Permeability could decrease if new

phases precipitate at pore throats and block fluid flow pathways, but predicted precipitation is so minor that it is unlikely to constrain flow in a porous sandstone.

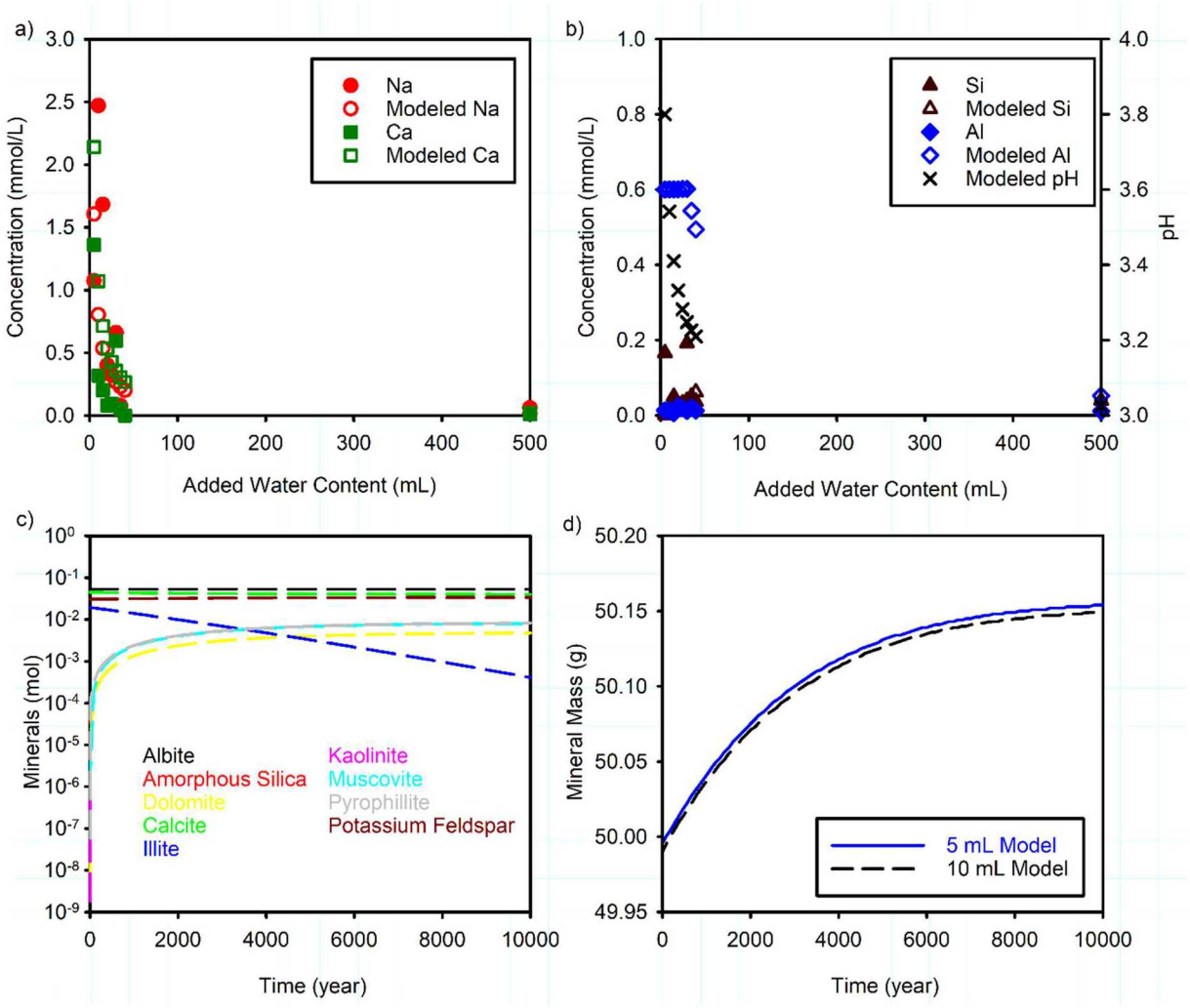

Figure 9. Predicted versus observed ion concentrations in $scCO_2$ with different added water contents for a) sodium and calcium; b) silica, aluminum, and predicted pH. c) Predicted changes in mineral concentration over 10000 years based on models calculated using 5 mL added DI H_2O input. d) Change in total mass over 10000 years based on models calculated using 5 mL and 10 mL added DI H_2O input.

3.5 Mechanical and chemical alteration of Boise Sandstone by hydrous $scCO_2$

In summary, the experiments conducted in this study document mechanical weakening caused by chemical reactions induced by water present as humidity in $scCO_2$. Our results show consistent weakening, but the extent of mechanical weakening is low and does not show clear correlations with the volume of added water. These mixed results between observed failure strengths, elastic moduli, scratch test properties, and ion concentrations make it difficult to determine clear relationships (Figure 5-7; Table 2, 3). Most notably, the experiments conducted in the presence of water without CO_2, and in dry $scCO_2$ do not alter the mechanical strength of the material (Figure 4; Table 3). Therefore, any observed weakening is caused by chemical reactions driven by water in the hydrous $scCO_2$ phase.

Observed weakening does not correlate between different testing methods either, as triaxial testing and scratch testing produce different results. The greatest weakening observed in triaxial testing is at $scCO_2$ with 20 mL added DI H_2O and $scCO_2$ with 500 mL DI H_2O. The greatest weakening observed in scratch toughness testing is at 5 mL added DI H_2O. $scCO_2$ with higher water contents does not induce significant weakening in triaxial testing, although scratch testing displays reduced toughness compared to unaltered samples. Regardless of the testing methods, weakening was observed only for samples reacted with hydrous $scCO_2$, leading to conclusions that this alteration mechanism is likely important at the time-scales needed for GCS.

Measurable ion concentrations were detected in water following its condensation out of hydrous $scCO_2$ indicating dissolution occurred during exposure, but the calculated dissolved rock mass represents a small percentage of the total rock mass (Figure 8; Table 4). The measured rock mass dissolved does not correlate with observed weakening, with the exception of $scCO_2$ with excess DI H_2O. Increased exposure time does not significantly increase dissolved rock

446 mass or observed weakening, indicating that the duration of experiment was not sufficient to
447 observe kinetically-controlled slow dissolution reactions in Boise Sandstone (Figure 6, 8; Table
448 2, 4). Because the chemical alteration is limited in the studied case, we did not observe
449 consistent relationships linking measured geomechanical properties to the added volume of
450 water. Additionally, natural sample-to-sample variability in composition, strength, mineralogy,
451 porosity, and grain structure likely obscured our results.
452 XRD results in unaltered Boise Sandstone show samples are primarily composed of
453 quartz (SiO_2), albite ($NaAlSi_3O_8$), microcline ($KAlSi_3O_8$), illite-smectite
454 ($(K,H_3O)(Al,Mg,Fe)_2(Si,Al)_4O_{10}[(OH)_2,(H_2O)]$), and calcite ($CaCO_3$). Post-exposure, solutions
455 show elevated levels of Ca^{2+}, likely from calcite dissolution. Calcite has the fastest dissolution
456 kinetics, compared to other minerals present. Detected Na^+ concentrations indicate albite
457 dissolution. For the sample with lowest added water, Ca^{2+} concentrations are higher than Na^+.
458 This suggests that at low water activity, the more favorable hydration energy of Ca^{2+} leads to the
459 higher mobility of Ca^{2+}, compared to Na^+ within the Boise Sandstone core. This has implications
460 for CO_2 storage sites, where preferential ion transport may be observed due to this phenomenon.
461 This warrants further research. As water activity is increased in our experiments, Na^+
462 concentrations are higher, suggesting that the competitive effect disappears. The presence of K^+
463 in solution could indicate the dissolution of microcline or illite-smectite. Both Mg^{2+} and Fe
464 indicate illite-smectite dissolution. Because K^+ levels are higher than Mg^{2+} and Fe, this suggests
465 dissolution of microcline in addition to illite-smectite. Silicon is present in greater quantities
466 than Mg^{2+} and Al, but lower compared to Na^+, Ca^{2+}, K^+, and Fe. Quartz dissolution rates reduce
467 with decreasing pH [*Dove*, 1995; *Dove and Rimstidt*, 1994], so Si in the system most likely
468 results from dissolution of feldspars and clay minerals. Both Al and Si are lower than expected

469 and do not display the same relationship with water content as the other ions. While
470 precipitation of amorphous phases cannot be ruled out, the results here indicate dissolution of
471 calcite and non-stoichiometric dissolution of illite-smectite, albite, and microcline.
472 Our experiments show that hydrous $scCO_2$ can induce minor mineral dissolution in Boise
473 Sandstone and lead to inconsistent weakening when deformed later. We observed similar
474 dissolution behavior to previous work in sandstones and simulated grain packs. Several studies
475 have observed dissolution of feldspars in the presence of water enriched with CO_2 [*P Lu et al.*,
476 2013; *P Lu et al.*, 2011; *Tutolo et al.*, 2015]. Dissolution of pure grain packs of anorthite, albite,
477 and microcline in CO_2 enriched fluids observed elevated levels Na^+, Ca^{2+}, and K^+ over Si and Al
478 levels, similar to our observations [*P Lu et al.*, 2013]. Calcite dissolution has been observed in
479 sandstones and limestones [*Hangx et al.*, 2013; *Huq et al.*, 2015; *Lamy□Chappuis et al.*, 2014;
480 *Le Guen et al.*, 2007]. The reactions observed in this study are similar to those reported in the
481 previous work, but the concentration of ions in this study are orders of magnitude lower than
482 previous work [*Credoz et al.*, 2011; *Huq et al.*, 2015; *Lamy□Chappuis et al.*, 2014; *P Lu et al.*,
483 2013; *P Lu et al.*, 2011; *Tutolo et al.*, 2015]. This difference could be caused by different
484 experimental conditions (temperature, time, flow rates, pressures and fluid-rock ratios), but is
485 likely a result of low water volumes used in this study. Previous work investigated chemo-
486 mechanical changes induced by CO_2 dissolved in water; while we investigated changes induced
487 by water dissolved in $scCO_2$. Water solubility is extremely low in $scCO_2$, so only small volumes
488 of water actually reached the samples despite excess available water. Consequently, mineral
489 dissolution was limited by the low availability of water. We observed dramatic weakening in
490 some experiments similar to previous work [*Lamy□Chappuis et al.*, 2014; *Le Guen et al.*, 2007;
491 *Luquot et al.*, 2012], but we also observed no change, similar to previous work [*Hangx et al.*,

2009; 2010; *Hangx et al.*, 2013]. Observed weakening must be dependent on individual pore structures in Boise Sandstone. Photomicrographs of unaltered samples show grains and pore throats are coated with microcrystalline quartz and quartz overgrowths (Figure 1), which would be resistant to dissolution and prevent any changes in geomechanical properties. Variations in flow pathways and availability of susceptible minerals at pore throats control potential weakening. The results presented here demonstrate that some minerals present in Boise Sandstone are likely to react in the presence of carbonic acid, and future experiments utilizing CO_2 enriched fluids could observe elevated levels of dissolution and mechanical weakening.

501 **5. Conclusions**

502 In geologic carbon storage projects, CO_2 is injected into subsurface reservoirs at pressure and
503 temperature conditions to ensure a supercritical state to maximize injectivity and storage. $scCO_2$
504 plumes displace native brines, but also interact with the brines and minerals and shift the
505 subsurface chemical steady-state or equilibrium conditions. At plume-brine interface, CO_2 and
506 water can partition into one another. The experiments conducted here demonstrate water present
507 as humidity in $scCO_2$ can induce chemical reactions and transport ions throughout the pore space
508 that could potentially impact reservoir integrity and hydraulic properties.
509
510 Samples of Boise Sandstone were exposed to hydrous supercritical CO_2 with varying amounts of
511 added water to investigate potential chemo-mechanical response during geologic carbon storage.
512 Previous work has investigated the effect of waters and brines enriched with CO_2, this study
513 investigated effects of supercritical CO_2 enriched with water. We exposed samples to
514 recirculating hydrous supercritical CO_2 with different amounts of available water at 70°C and
515 13.8 MPa CO_2 pressure for 24-hour and 168-hour time periods. Post exposure, mechanical
516 changes due to exposure were investigated using triaxial testing and surface scratch testing, and
517 induced chemical reactions were determined by sampling water for dissolved ions. Weakening
518 due to exposure to hydrous supercritical CO_2 was observed in testing, but the results do not show
519 clear trends with respect to water content. For scratch testing, samples exposed to 5 mL added
520 DI H_2O supercritical CO_2 show the greatest weakening, and in triaxial testing, samples exposed
521 to 20 mL and 500 mL added DI H_2O supercritical CO_2 showed the greatest weakening.
522 Experiments conducted on samples exposed to supercritical CO_2 with excess water show
523 weakening with increasing mean stress. Measurable amounts of sodium, calcium, potassium,

magnesium, iron, silicon, and aluminum are observed, indicating dissolution of calcite, albite, microcline, and illite-smectite. The highest levels of observed dissolution did not coincide with greater weakening in either triaxial or scratch testing. Results are dominated by sample to sample variability and suggest that individual pore scale structures control chemically induced weakening as many grains are lined with chemically stable quartz cementing phases. This study does demonstrate that water can partition into supercritical CO_2 and induce chemical alterations in reactive minerals that could impact geologic carbon storage projects. However, water saturation is low in supercritical CO_2, making it unlikely to see significant changes in a quartz cemented sandstone in storage reservoirs. Sandstones with more susceptible cementing phases could be adversely affected by the presence of hydrous supercritical CO_2.

Acknowledgments

This work was supported as part of the Center for Frontiers in Subsurface Energy Security, an Energy Frontier Research Center funded by the U.S. Department of Energy, Office of Science, Basic Energy Sciences under Award # DE-SC0001114. Sandia National Laboratories is a multimission laboratory managed and operated by National Technology and Engineering Solutions of Sandia, LLC., a wholly owned subsidiary of Honeywell International, Inc., for the U.S. Department of Energy's National Nuclear Security Administration under contract DE-NA-0003525.

This paper describes objective technical results and analysis. Any subjective views or opinions that might be expressed in the paper do not necessarily represent the views of the U.S. Department of Energy or the United States Government.

Disclaimer

This paper describes objective technical results and analysis. Any subjective views or opinions that might be expressed in the paper do not necessarily represent the views of the U.S. Department of Energy or the United States Government.

6. References

Alemu, B. L., P. Aagaard, I. A. Munz, and E. Skurtveit (2011), Caprock interaction with CO 2: a laboratory study of reactivity of shale with supercritical CO 2 and brine, *Applied Geochemistry*, *26*(12), 1975-1989.

Aman, M., D. N. Espinoza, A. G. Ilgen, J. R. Major, P. Eichhubl, and T. A. Dewers (2018), CO2□induced chemo□mechanical alteration in reservoir rocks assessed via batch reaction experiments and scratch testing, *Greenhouse Gases: Science and Technology*, *8*(1), 133-149.

Bethke, C. (2008), Geochemical and biogeochemical reaction modeling, Cambridge University Press, *Cambridge (UK)*.

Castellanza, R., and R. Nova (2004), Oedometric tests on artificially weathered carbonatic soft rocks, *Journal of geotechnical and geoenvironmental engineering*, *130*(7), 728-739.

Chen, Y., and S. L. Brantley (1997), Temperature-and pH-dependence of albite dissolution rate at acid pH, *Chemical Geology*, *135*(3-4), 275-290.

Ciantia, M. O., R. Castellanza, and C. di Prisco (2015), Experimental study on the water-induced weakening of calcarenites, *Rock Mechanics and Rock Engineering*, *48*(2), 441-461.

Ciantia, M. O., and T. Hueckel (2013), Weathering of submerged stressed calcarenites: chemo-mechanical coupling mechanisms, *Géotechnique*, *63*(9), 768-785.

Credoz, A., O. Bildstein, M. Jullien, J. Raynal, L. Trotignon, and O. Pokrovsky (2011), Mixed-layer illite–smectite reactivity in acidified solutions: Implications for clayey caprock stability in CO 2 geological storage, *Applied Clay Science*, *53*(3), 402-408.

Dove, P. (1995), Kinetic and thermodynamic controls on silica reactivity in weathering environments, *Reviews in Mineralogy and Geochemistry*, *31*(1), 235-290.

Dove, P., and J. Rimstidt (1994), Silica-water interactions, *Reviews in Mineralogy and Geochemistry*, *29*(1), 259-308.

Gajo, A., F. Cecinato, and T. Hueckel (2015), A micro-scale inspired chemo-mechanical model of bonded geomaterials, *International Journal of Rock Mechanics and Mining Sciences*, *80*, 425-438.

Garcia, D. J., H. Shao, Y. Hu, J. R. Ray, and Y.-S. Jun (2012), Supercritical CO 2–brine induced dissolution, swelling, and secondary mineral formation on phlogopite surfaces at 75–95° C and 75 atm, *Energy & Environmental Science*, *5*(2), 5758-5767.

Hangx, S., C. Spiers, and C. Peach (2009), The mechanical behavior of anhydrite and the effect of CO 2 injection, *Energy Procedia*, *1*(1), 3485-3492.

584 Hangx, S., C. Spiers, and C. Peach (2010), Creep of simulated reservoir sands and coupled
585 chemical□mechanical effects of CO2 injection, *Journal of Geophysical Research: Solid Earth*,
586 *115*(B9).

587 Hangx, S., A. van der Linden, F. Marcelis, and A. Bauer (2013), The effect of CO2 on the
588 mechanical properties of the Captain Sandstone: Geological storage of CO2 at the Goldeneye
589 field (UK), *International Journal of Greenhouse Gas Control*, *19*, 609-619.

590 Huq, F., S. B. Haderlein, O. A. Cirpka, M. Nowak, P. Blum, and P. Grathwohl (2015), Flow-
591 through experiments on water–rock interactions in a sandstone caused by CO 2 injection at
592 pressures and temperatures mimicking reservoir conditions, *Applied Geochemistry*, *58*, 136-146.

593 Kim, D., C. Peters, and W. Lindquist (2011), Upscaling geochemical reaction rates
594 accompanying acidic CO2□saturated brine flow in sandstone aquifers, *Water Resources*
595 *Research*, *47*(1).

596 Koide, H., Y. Tazaki, Y. Noguchi, M. Iijima, K. Ito, and Y. Shindo (1993), Carbon dioxide
597 injection into useless aquifers and recovery of natural gas dissolved in fossil water, *Energy*
598 *conversion and management*, *34*(9), 921-924.

599 Lamy□Chappuis, B., D. Angus, Q. Fisher, C. Grattoni, and B. W. Yardley (2014), Rapid
600 porosity and permeability changes of calcareous sandstone due to CO2□enriched brine injection,
601 *Geophysical Research Letters*, *41*(2), 399-406.

602 Le Guen, Y., F. Renard, R. Hellmann, E. Brosse, M. Collombet, D. Tisserand, and J. P. Gratier
603 (2007), Enhanced deformation of limestone and sandstone in the presence of high fluids, *Journal*
604 *of Geophysical Research: Solid Earth*, *112*(B5).

605 Liu, F., P. Lu, C. Griffith, S. W. Hedges, Y. Soong, H. Hellevang, and C. Zhu (2012), CO 2–
606 brine–caprock interaction: reactivity experiments on Eau Claire shale and a review of relevant
607 literature, *International Journal of Greenhouse Gas Control*, *7*, 153-167.

608 Lu, J., P. J. Mickler, J.-P. Nicot, C. Yang, and K. D. Romanak (2014), Geochemical impact of
609 oxygen on siliciclastic carbon storage reservoirs, *International Journal of Greenhouse Gas*
610 *Control*, *21*, 214-231.

611 Lu, P., Q. Fu, W. E. Seyfried Jr, S. W. Hedges, Y. Soong, K. Jones, and C. Zhu (2013), Coupled
612 alkali feldspar dissolution and secondary mineral precipitation in batch systems–2: New
613 experiments with supercritical CO2 and implications for carbon sequestration, *Applied*
614 *geochemistry*, *30*, 75-90.

615 Lu, P., Q. Fu, W. E. Seyfried Jr, A. Hereford, and C. Zhu (2011), Navajo Sandstone–brine–CO2
616 interaction: implications for geological carbon sequestration, *Environmental Earth Sciences*,
617 *62*(1), 101-118.

618 Luquot, L., M. Andreani, P. Gouze, and P. Camps (2012), CO 2 percolation experiment through
619 chlorite/zeolite-rich sandstone (Pretty Hill Formation–Otway Basin–Australia), *Chemical*
620 *geology*, *294*, 75-88.

621 Major, J. R. (2018), Natural fractures in mucrocks and top seal integrity: Insights from
622 diagenesis, rock mechanics, and modeling applied to CO2 sequestration and hydrocarbon
623 exploration, 302 pp, The University of Texas at Austin.

624 Pacala, S., and R. Socolow (2004), Stabilization wedges: solving the climate problem for the
625 next 50 years with current technologies, *science*, *305*(5686), 968-972.

626 Rosenbauer, R. J., T. Koksalan, and J. L. Palandri (2005), Experimental investigation of CO 2–
627 brine–rock interactions at elevated temperature and pressure: implications for CO 2 sequestration
628 in deep-saline aquifers, *Fuel processing technology*, *86*(14), 1581-1597.

629 Rutqvist, J. (2012), The geomechanics of CO2 storage in deep sedimentary formations,
630 *Geotechnical and Geological Engineering*, *30*(3), 525-551.

631 Shao, H., J. R. Ray, and Y.-S. Jun (2010), Dissolution and precipitation of clay minerals under
632 geologic CO2 sequestration conditions: CO2− brine− phlogopite interactions, *Environmental*
633 *science & technology*, *44*(15), 5999-6005.

634 Spycher, N., K. Pruess, and J. Ennis-King (2003), CO 2-H 2 O mixtures in the geological
635 sequestration of CO 2. I. Assessment and calculation of mutual solubilities from 12 to 100 C and
636 up to 600 bar, *Geochimica et cosmochimica acta*, *67*(16), 3015-3031.

637 Tutolo, B. M., A. J. Luhmann, X.-Z. Kong, M. O. Saar, and W. E. Seyfried (2015), CO 2
638 sequestration in feldspar-rich sandstone: coupled evolution of fluid chemistry, mineral reaction
639 rates, and hydrogeochemical properties, *Geochimica et Cosmochimica Acta*, *160*, 132-154.

640 Xu, T., Y. K. Kharaka, C. Doughty, B. M. Freifeld, and T. M. Daley (2010), Reactive transport
641 modeling to study changes in water chemistry induced by CO2 injection at the Frio-I Brine Pilot,
642 *Chemical Geology*, *271*(3-4), 153-164.

643 Zhu, W., and T. f. Wong (1997), The transition from brittle faulting to cataclastic flow:
644 Permeability evolution, *Journal of Geophysical Research: Solid Earth*, *102*(B2), 3027-3041.

645 Zoback, M. D., and S. M. Gorelick (2012), Earthquake triggering and large-scale geologic
646 storage of carbon dioxide, *Proceedings of the National Academy of Sciences*, *109*(26), 10164-
647 10168.
648
649